Hexagonal Monolayer Ice without Shared Edges

Xin Zhang,[1,*] Ji-Yu Xu,[2,*] Yu-Bing Tu,[1] Kai Sun,[1] Min-Long Tao,[1] Zu-Hong Xiong,[1] Ke-Hui Wu,[2] Jun-Zhong Wang,[1,†] Qi-Kun Xue,[3] and Sheng Meng[2,‡]

[1]*School of Physical Science and Technology, Southwest University, Chongqing 400715, China*
[2]*Institute of Physics, Chinese Academy of Sciences, Beijing 100190, China*
[3]*Department of Physics, Tsinghua University, Beijing 100084, China*

(Received 24 May 2018; revised manuscript received 29 August 2018; published 21 December 2018)

When adsorbed on solids, water molecules are usually arranged into a honeycomb hydrogen-bond network. Here we report the discovery of a novel monolayer ice built exclusively from water hexamers but without shared edges, distinct from all conventional ice phases. Water grown on graphite crystalizes into a robust monolayer ice after annealing, attaining an exceedingly high density of 0.134 $Å^{-2}$. Unlike chemisorbed ice on metal surfaces, the ice monolayer can translate and rotate on graphite terraces and grow across steps, confirming its two-dimensional nature. First-principles calculations identify the monolayer ice structure as a robust self-assembly of closely packed water hexamers without edge sharing, whose stability is maintained by maximizing the number of intralayer hydrogen bonds on inert surfaces.

DOI: 10.1103/PhysRevLett.121.256001

Ice structures on solid surfaces have a grand importance in a wide range of natural and technological processes such as protein folding, lubrication, corrosion, electrochemistry, and heterogeneous catalysis [1,2]. The structure of interfacial water is crucial for understanding and controlling the wettability of water [3,4]. On metal surfaces, various ice structures have been found and were previously interpreted in terms of the "icelike" bilayer model; namely, water molecules adopt a puckered hexagonal network with oxygen atoms located at two distinct heights, resembling the basal plane of hexagonal ice I_h [5–7]. However, recent experimental studies based on scanning tunneling microscopy (STM) demonstrate that there are a variety of disorders and distortions in water wetting layers. Consequently, unconventional nonhexagonal ice layers have been found on noble Pt(111) and Pd(111) surfaces [8–14], inconsistent with the long-standing bilayer model. The formation of these ice phases was attributed to the delicate balance between the water-water and water-metal interactions [3]. On reactive Ru (0001) surface, water dissociation took place and mixed water-hydroxyls were observed [15,16]. In the case of insulating surfaces, a distinct monolayer ice containing Bjerrum *D*-type defects was found on a NaCl film [17]. Despite intensive studies, precise structures of water on inert surfaces have been elusive.

Graphite-graphene is a model system for studying interfacial water thanks to the homogeneity and morphological flatness [18]. In the past decades, a large number of investigations have been carried out to understand the adsorption, wetting, and crystallization kinetics of ice films on graphite-graphene surfaces by means of spectroscopic or diffraction methods [19,20], as well as theoretical simulations [21,22]. It has been shown that thin films of amorphous solid water (ASW) can be formed by vapor deposition of water molecules onto a cold graphite surface below 100 K. Deposition between 140 and 180 K results in the formation of bilayer ice at the water-graphite interface. Dewetting of ASW takes place between 140 and 180 K, depending on the film's thickness [23,24]. However, detailed arrangement of water molecules at the interface remains controversial, mainly because of the lack of direct structural characterization at the molecular level. It is a significant challenge to determine the structure of the water-graphite interface with high precision, for the sake of fundamental understanding of water-graphite interaction.

Here we report that the water layer crystallizes into a robust hexagonal monolayer ice with an exceedingly high density (0.134 $Å^{-2}$) after annealing to ~160 K. High-resolution STM analyses aided by first-principles calculations clearly demonstrate that the monolayer ice is built exclusively from closely packed water hexamers but without shared edges, in sharp contrast to conventional honeycomb ice structures. Furthermore, the weakly bound monolayer ice sheets can be manipulated, with multiple orientations with respect to the graphite lattice resulting in various moiré patterns.

The experiments were performed in a Unisoku low-temperature STM system with a base pressure of 1.2×10^{-10} Torr. The substrate used was a flake of high orientated pyrolytic graphite (HOPG). The ultrapure H_2O (for ultratrace analysis) from Sigma Aldrich was further purified in vacuum by freeze-thaw cycles to remove the remaining impurities. Ice films were grown by directing water vapor onto the HOPG surface at 80 K through a dosing tube. The pressure during deposition was typically kept at 1.0×10^{-4} Torr, which results in a very thick ASW

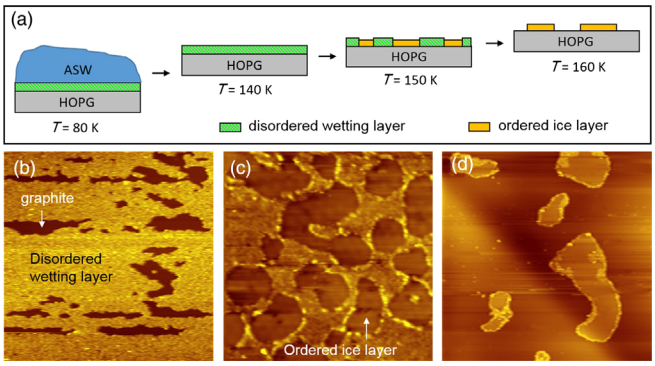

FIG. 1. (a) Schematic diagram showing the sublimation of amorphous solid water (ASW) and the subsequent crystallization of the water wetting layer driven by annealing to higher temperatures. (b) Morphology of water wetting layer after the sublimation of ASW. The cracks and voids existing in the wetting layer make the graphite substrate exposed, 200×200 nm^2, $U_s = 2.8$ V, $I_t = 28$ pA. (c) Crystallization of the disordered wetting layer leads to the formation of small domains of ordered ice layer by annealing to 150 K, 100×100 nm^2, $U_s = 3.0$ V, $I_t = 28$ pA. (d) Further annealing to 160 K results in the total sublimation of disordered wetting layer and the coalescence of small domains of ordered monolayer ice, 300×300 nm^2, $U_s = 3.0$ V, $I_t = 30$ pA.

film on top of the wetting layer. Annealing to ~140 K (measured at the sample holder) led to the complete sublimation of ASW and the exposure of the wetting layer. Further annealing to 150 K caused the crystallization of the wetting layer into small patches of ordered monolayer ice. When the temperature rises to 160 K, nearly all the disordered wetting layer sublimated, leaving the 2D crystalline ice islands on the graphite surface [Fig. 1(a)]. All the STM images were acquired with a tungsten tip at 78 or 4.7 K.

The morphology of the water layer after evaporation of ASW is shown in Fig. 1(b), where no structural order can be found. Instead, the wetting layer contains some cracks and voids, exposing partial graphite surface. Figure 1(c) shows the patches of ordered monolayer ice with sizes ranging from a few to tens of nanometers. Annealing at 160 K results in the desorption of disordered water layers and the coalescence of crystalline patches into large 2D islands ranging from tens to hundreds of nanometers [Fig. 1(d)]. The 2D ice islands display an apparent height of ~1.6 Å in STM, close to the thickness of the water wetting layer (0.8–1.6 Å) on Pd(111) and Ru(0001) [9,14]. In addition, some water molecules decorating the island edges have a larger height and disordered arrangement, suggesting that they are the residual of ASW. Because of the poor conductivity of disordered ice, a high-bias voltage (>3 V) was used in the STM scanning to avoid tip collision, which has no influence on the topological structure of crystalline ice (see Supplemental Material, Fig. S1 [25]).

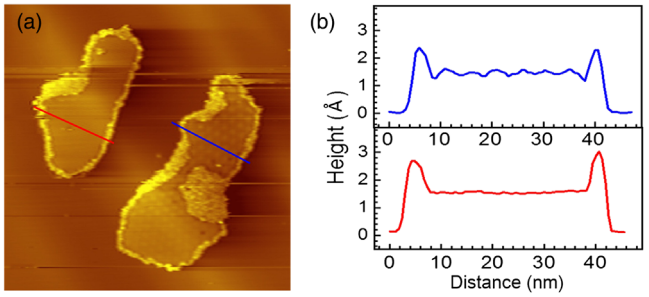

FIG. 2. (a) Coexistence of two monolayer ice islands with different orientations on the same graphite surface, 150×150 nm^2, $U_s = +3.5$ V, $I_t = 28$ pA. (b) Height profiles along the blue and red lines shown in (a), revealing distinct fluctuation amplitudes and moiré periodicities.

Because of lattice mismatch and misorientation, moiré patterns with a variety of periodicity can be observed. Figure 2(a) shows two monolayer ice islands with different moiré patterns. The left-hand ice island reveals a moiré superstructure with ~24 Å periodicity and ~0.1 Å corrugation due to the large misorientation (~5°) with respect to the graphite lattice, while the right-hand ice island shows a moiré pattern with ~46 Å periodicity and ~0.2 Å corrugation with a smaller misorientation (~3°) [Fig. 2(b)]. The emergence of various moiré patterns implies that the monolayer ice might be out of registry with graphite lattice.

Figure 3 displays the high-resolution STM images of monolayer ice with a small misorientation (~2.0°). A well-defined hexagonal moiré pattern with ~50 Å periodicity can be clearly seen [Fig. 3(b)]. The lattice constant of the ice monolayer is 7.2 ± 0.2 Å, approximately 3 times that of graphite (2.46 Å). The former is significantly larger than that of the commensurate $(\sqrt{3} \times \sqrt{3}) - R30°$ hexagonal ice on Pt(111), 4.8 Å [5]. As revealed by the enlarged image [Fig. 3(c)], monolayer ice is composed of water rings, distinct from the honeycomb structure of hexagonal ice. In particular, there is a "flat" water ring revealing its hexagonal shape (marked by the green dot at the frame center). Because of mismatch and misorientation to graphite substrate, 6, 12, and 18 seemingly tilted water rings are located at the first, second, and third neighboring positions to the flat ring in the STM image, respectively. The tilted magnitude becomes stronger in the molecules which are farther away from the flat water ring [Fig. 3(c)]. When the bias was changed to −1.3 V (see Supplemental Material, Fig. S2(b) [25]), nearly all the water rings revealed a flat hexagon with side-by-side arrangement in the STM image. The STM images of the monolayer ice are dependent on the bias voltage. However, when the bias voltage was changed back to +1.3 V, the monolayer ice exhibited the same tilted hexagons again, indicating the hexagonal topological structure of ice has not been modified by the negative voltage. Thus, each hexagon can be attributed to a water hexamer. We note that the six water molecules comprising a

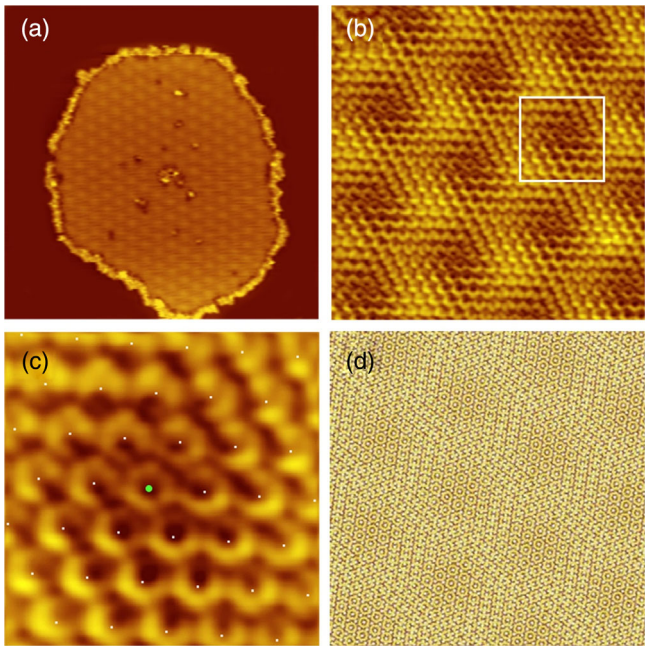

FIG. 3. High-resolution STM images of the hexagonal monolayer ice without shared edges. (a) Typical monolayer ice island with small misorientation (~2.0°) relative to the graphite lattice recorded at 78 K, 100×100 nm^2, $U_s = +3.0$ V, $I_t = 28$ pA. (b) Moiré pattern revealed by the monolayer ice, 15×15 nm^2, $U_s = +1.3$ V, $I_t = 29$ pA. (c) Enlarged images (4×4 nm^2) corresponding to the box region in (b) acquired at +1.3 V ($I_t = 29$ pA). The green dots represent the center of the "flat" hexagonal ring. (d) Simulated moiré pattern from molecular mechanics simulations corresponding to that with ~50 Å periodicity in (b).

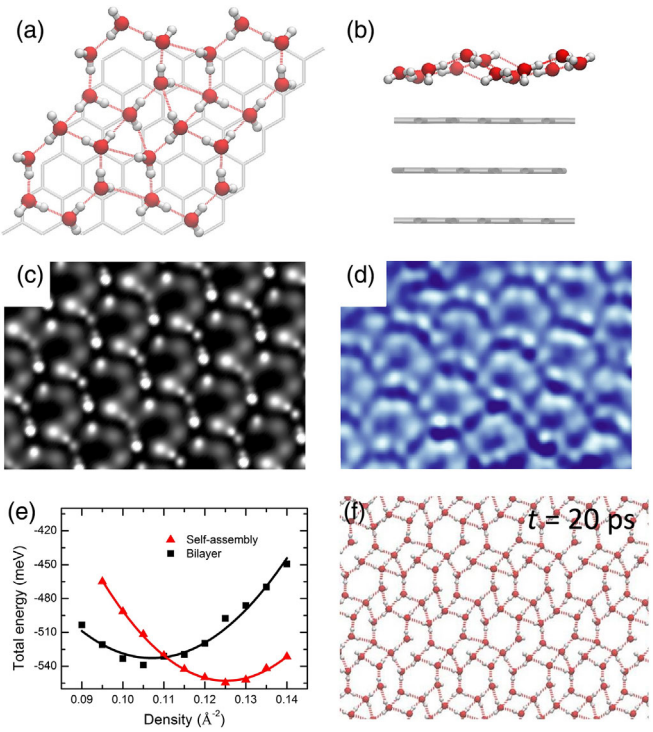

FIG. 4. Optimized structure for the monolayer ice on graphite. (a) Top and (b) side views of the optimized geometry of the monolayer ice from DFT calculations. (c) Simulated STM image of the monolayer ice. (d) Experimental STM image of the monolayer ice recorded at liquid helium temperature ($T = 4.7$ K, 35×25 Å^2), $U_s = 1.2$ V, $I_t = 29$ pA. Each water hexamer reveals six protrusions with different contrast, corresponding to different heights of the six water molecules. (e) Total binding energy of the monolayer ice and ice bilayer as a function of water density. (f) A typical snapshot of monolayer ice during AIMD simulation. There is no structural change in the monolayer ice during the MD simulation of 20 ps. Color code is C, gray; O, red; H, white; hydrogen bond, red dotted line.

hexamer can be clearly resolved at liquid helium temperature; see Fig. 4(d). Additionally, we have modeled the moiré pattern of 2D ice on a graphite lattice in molecular mechanics simulations. We adopt the experimental values of the graphite lattice (2.46 Å) and the lattice constant of 7.2 Å as measured in STM for the 2D ice structure. The 2D ice structure is superimposed on the graphite lattice with a misorientation angle of ~2°. Then we optimize the 2D ice adsorption structure via molecular mechanics simulations with empirical carbon-water interactions and TIP4P water interactions. The moiré patterns with a periodicity of about 50 Å can be clearly obtained in our simulations [Fig. 3(d)], which agree well with the patterns observed in experiments [Fig. 3(b)]. The packing density of water in this monolayer is 0.134 Å^{-2}, the highest among the reported 2D ice layers on surfaces (see Supplemental Material, Fig. S3 [25]).

In order to fully understand the detailed structure of the monolayer ice, we perform density functional theory (DFT) calculations and *ab initio* molecular dynamics (AIMD) simulations using CP2K (see Supplemental Material for details [25]). Because of the large periodicity and great complexity of different moiré patterns, we focus on the arrangement of the water overlayer without misorientation and mismatch to the graphite substrate for simplicity. A (6×6) supercell with a lattice constant of 14.76 Å is adopted. The graphite substrate was treated as three graphene layers. To avoid artifacts on the interactions between periodic images, the vacuum layer of 20 Å is used. Twenty-four water molecules in the cell give rise to a packing density of 0.127 Å^{-2}, close to the highest packing density of water found in experiment.

In Figs. 4(a) and 4(b) we show the top and side views of the optimized geometry of the monolayer ice obtained from first-principles calculations. After extensive structural search and optimization, water molecules form hexagonal rings tilted in the same direction with a height difference of 1.5 Å for the highest and lowest oxygen atoms. All the water hexamers are interlinked through hydrogen bonds without edge sharing, which is consistent with experimental observations. The total binding energy for the water monolayer supported on graphite is 552 meV per water molecule, comprising the intralayer hydrogen-bonding

TABLE I. The total binding energy (E_{total}), intralayer binding energy (E_{intra}), and adsorption energy (E_{ads}) for ice layers on graphite.

Structure	E_{total} (meV)	E_{intra} (meV)	E_{ads} (meV)
Self-assembly ice	552	475	77
H-down (bilayer)	499	410	89
H-up (bilayer)	487	411	76

energy of 475 meV and adsorption energy on graphite of 77 meV. Compared with conventional ice bilayers [21,45], the 2D monolayer ice is stable and robust at the density of 0.127 $Å^{-2}$ (see Table I and Supplemental Material, Fig. S4 [25]).

We simulate the STM image of the proposed ice structure, as displayed in Fig. 4(c). The different contrast of individual water molecules reflects the variations in height. Each water hexamer reveals six protrusions with different contrast, corresponding to different heights of the six water molecules. The simulated image is in excellent agreement with the experimental image of monolayer ice acquired at the liquid helium temperature (4.7 K, sample holder temperature) shown in Fig. 4(d). The similarity and consistency strongly suggest that water hexamers are the basic building blocks for the monolayer ice, exhibiting various moiré patterns when connected and adsorbed on graphite.

To simulate the effect of the graphite substrate without lattice registry, we model graphite as an external 9-3 potential imposed on oxygen atoms, $E = \varepsilon[\frac{2}{15}(\sigma^9/z^9) - (\sigma^3/z^3)]$, where ε takes 100 meV and σ takes 4.1 Å. Thus the formation energy of water layers on graphite at an arbitrary density can be calculated. As shown in Fig. 4(e), the monolayer ice is stable at the high density region, while ice bilayers are stable at the small density region. In addition, the energy difference between the two ice phases at 0.134 $Å^{-2}$ is nearly 70 meV, nicely explaining the emergence of the 2D monolayer ice in experiment. The energetic order has been further confirmed in calculations with different functionals (see Supplemental Material, Fig. S5 [25]). Further analysis demonstrates that the hydrogen bonds within water hexamers are very strong (~300 meV) and nearly constant as water density increases, while the hydrogen bonds between water hexamers are weak as a result of geometry constraints and small O─H…O angles, whose strength increases from 100 to 200 meV as density increases (see Supplemental Material, Fig. S6(b) [25]). The increase of binding strength between water hexamers shows the effect of maximizing the number of intralayer hydrogen bonds. This fact implies that the novel ice monolayer can be formed by self-assembly of water hexamers, a robust ice building block on inert surfaces such as graphite. Compared with bulk ice, the novel 2D monolayer ice is a metastable phase at high adsorption density of water. However, the formation of bulk ice can be kinetically blocked by a large energy barrier in specific conditions. We note that the ice structures found in our experiments are in the form of islands; similar ice islands have been observed in the literature [19,23]. The small adsorption energy of 77 meV also indicates that the interactions between water hexamers and graphite are weak. These weakly bound hexamers can easily assemble into the monolayer ice observed in STM.

We note that the self-assembly ice looks similar to a layer of ice II seen along the c axis. Ice II is a stable phase under a pressure of 0.2–0.6 GPa below 200 K, whose unit cell consists of two nonequivalent units—flat and chair-form water hexamers (see Supplemental Material, Fig. S7 [25]). Thus the self-assembly ice can be considered as a cut of ice II strongly confined in two dimensions with varied molecular configurations. We estimate that the graphite substrate can impose a pressure up to 0.8 GPa to the adsorbed ice layer (see Supplemental Material, Fig. S8 [25]). Both ice layers exhibit the same trend and minimum position in the energy profiles as a function of density (see Supplemental Material, Fig. S9 [25]). The self-assembly ice is about 10 meV/H_2O more stable, which is attributed to more in-plane hydrogen bonds formed by flat hexamers to further stabilize the ice layer. Considering these similarities, we think the self-assembly ice is a variation of ice II in two dimensions.

Further AIMD simulations reveal that at the packing density of 0.127 $Å^{-2}$, non-edge-sharing monolayer ice remains stable over 20 ps simulation, while the ice bilayer structures collapse in 1 ps. A snapshot of the simulation is shown in Fig. 4(f), where we see that each water hexamer is interconnected by hydrogen bonds with adjacent water hexamers. The AIMD simulations include the effects of both bonding energy and vibrational entropy, which demonstrates the thermodynamic stability of self-assembly ice. Considering the small contribution of residual entropy in 2D ices (~4 meV; see Supplemental Material [25]), the monolayer ice comprising non-edge-sharing water hexamers is thermodynamically stable on graphite.

Because of the inertness of the graphite surface and weak water-graphite interaction, the ice monolayer takes its own lattice and orientation without pinning commensurately to the substrate, as reported on metal surfaces. As a result, the individual ice islands on the same graphite surface have different orientations and show distinct moiré patterns. The misorientation angles range from 0 to 12 degrees according to STM data. Based on our statistical analysis, 40% ice islands show a small misorientation angle (0–2.5 deg); 45% ice islands have an intermediate misorientation angle (2.5–5.0 deg); only 15% ice islands reveal a large misorientation angle (5–12 deg). We also observed monolayer ice structures with a misorientation angle of $4.0 \pm 0.5°$ with respect to the graphite lattice (see Supplemental Material, Fig. S10 [25]). It was observed that

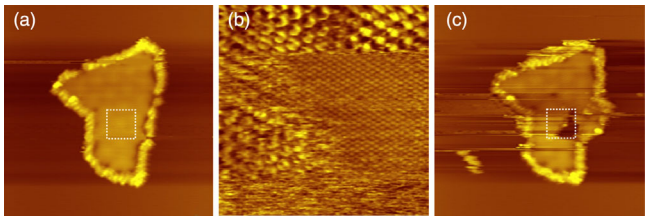

FIG. 5. Artificial voids in the monolayer ice island induced by a STM tip. (a) Intact monolayer ice island surrounded by a few ASW, 60×60 nm^2, $U_s = 3.0$ V, $I_t = 30$ pA. (b) Enlarged scanning of the box region in (a) at low-bias voltage, 9×9 nm^2, $U_s = 0.1$ V $I_t = 30$ pA. The STM tip penetrated the monolayer ice and made the graphite surface exposed. (c) Rescanning the monolayer ice island after the penetration, 60×60 nm^2, $U_s = 3.0$ V, $I_t = 30$ pA. A vacancy void can be found in the box region. Some water molecules were pushed to the right side of the ice island, some molecules are dragged out by the STM tip to the lower left.

the tilted water hexamers reveal a similar topography as that appearing in Fig. 3.

It was noticed that artificial voids in ice islands can be created by a STM tip with low-bias scanning (Fig. 5). By reducing the bias voltage to 0.1 V while keeping the tunneling current at 30 pA, the monolayer ice was penetrated by the STM tip. A patch of monolayer ice was dragged out and the bare graphite lattice became visible [Fig. 5(c)]. It is also interesting to note that the monolayer ice island may grow across the steps of graphite without being broken up, affirming the flexibility and toughness of monolayer ice (see Supplemental Material, Fig. S11 [25]). In addition, the monolayer ice islands could be rotated and moved from one place to another by STM tips, when changing the scanning direction (see Supplemental Material, Fig. S12 [25]), further verifying the relative stability of the monolayer ice, in a similar manner as 2D graphene. This study will have far-reaching implications for controlling ice structures on chemically inert substrates.

This work was supported by the National Natural Science Foundation of China (Grants No. 11574253, No. 11374242, No. 11604269, and No. 11474328), Ministry of Science and Technology (Grants No. 2016YFA0300902 and No. 2015CB921001).

*These authors contributed equally to this work.
†Corresponding author.
jzwangcn@swu.edu.cn
‡Corresponding author.
smeng@iphy.ac.cn

[1] M. A. Henderson, Surf. Sci. Rep. **46**, 1 (2002).
[2] A. Verdaguer, G. M. Sacha, H. Bluhm, and M. Salmeron, Chem. Rev. **106**, 1478 (2006).
[3] S. Maier and M. Salmeron, Acc. Chem. Res. **48**, 2783 (2015).
[4] A. Hodgson and S. Haq, Surf. Sci. Rep. **64**, 381 (2009); J. Carrasco, A. Hodgson, and A. Michaelides, Nat. Mater. **11**, 667 (2012); K. Koga, X. C. Zeng, and H. Tanaka, Phys. Rev. Lett. **79**, 5262 (1997); J. Bai and X. C. Zeng, Proc. Natl. Acad. Sci. U.S.A. **109**, 21240 (2012); D. T. Limmer, A. P. Willard, P. Madden, and D. Chandler, Proc. Natl. Acad. Sci. U.S.A. **110**, 4200 (2013).
[5] H. Ogasawara, B. Brena, D. Nordlund, M. Nyberg, A. Pelmenschikov, L. G. M. Pettersson, and A. Nilsson, Phys. Rev. Lett. **89**, 276102 (2002).
[6] C. Y. Ruan, V. A. Lobastov, F. Vigliotti, S. Y. Chen, and A. H. Zewail, Science **304**, 80 (2004).
[7] F. McBride, G. R. Darling, K. Pussi, and A. Hodgson, Phys. Rev. Lett. **106**, 226101 (2011).
[8] J. Cerda, A. Michaelides, M. L. Bocquet, P. J. Feibelman, T. Mitsui, M. Rose, E. Fomin, and M. Salmeron, Phys. Rev. Lett. **93**, 116101 (2004).
[9] M. Tatarkhanov, D. F. Ogletree, F. Rose, T. Mitsui, E. Fomin, S. Maier, M. Rose, J. I. Cerda, and M. Salmeron, J. Am. Chem. Soc. **131**, 18425 (2009).
[10] S. Nie, P. J. Feibelman, N. C. Bartelt, and K. Thürmer, Phys. Rev. Lett. **105**, 026102 (2010).
[11] S. Standop, A. Redinger, M. Morgenstern, T. Michely, and C. Busse, Phys. Rev. B **82**, 161412 (2010).
[12] S. Maier, I. Stass, T. Mitsui, P. J. Feibelman, K. Thürmer, and M. Salmeron, Phys. Rev. B **85**, 155434 (2012).
[13] K. Thuermer, S. Nie, P. J. Feibelman, and N. C. Bartelt, J. Chem. Phys. **141**, 18C520 (2014).
[14] S. Maier, B. A. J. Lechner, G. A. Somorjai, and M. Salmeron, J. Am. Chem. Soc. **138**, 3145 (2016).
[15] P. J. Feibelman, Science **295**, 99 (2002).
[16] S. Maier, I. Stass, J. I. Cerda, and M. Salmeron, Phys. Rev. Lett. **112**, 126101 (2014).
[17] J. Chen, J. Guo, X. Meng, J. Peng, J. Sheng, L. Xu, Y. Jiang, X.-Z. Li, and E.-G. Wang, Nat. Commun. **5**, 4056 (2014).
[18] Y. Zheng, C. Su, J. Lu, and K. P. Loh, Angew. Chem., Int. Ed. **52**, 8708 (2013); Z. Li, Y. Wang, A. Kozbial, G. Shenoy, F. Zhou, R. McGinley, P. Ireland, B. Morganstein, A. Kunkel, S. P. Surwade, L. Li, and H. Liu, Nat. Mater. **12**, 925 (2013); J. Rafiee, X. Mi, H. Gullapalli, A. V. Thomas, F. Yavari, Y. F. Shi, P. M. Ajayan, and N. A. Koratkar, Nat. Mater. **11**, 217 (2012); G. Algara-Siller, O. Lehtinen, F. C. Wang, R. R. Nair, U. Kaiser, H. A. Wu, A. K. Geim, and I. V. Grigorieva, Nature (London) **519**, 443 (2015).
[19] G. A. Kimmel, J. Matthiesen, M. Baer, C. J. Mundy, N. G. Petrik, R. S. Smith, Z. Dohnalek, and B. D. Kay, J. Am. Chem. Soc. **131**, 12838 (2009).
[20] D.-S. Yang and A. H. Zewail, Proc. Natl. Acad. Sci. U.S.A. **106**, 4122 (2009); H. Zhou, P. Ganesh, V. Presser, M. C. F. Wander, P. Fenter, P. R. C. Kent, D.-e. Jiang, A. A. Chialvo, J. McDonough, K. L. Shuford, and Y. Gogotsi, Phys. Rev. B **85**, 035406 (2012); D. Chakarov and B. Kasemo, Phys. Rev. Lett. **81**, 5181 (1998); R. S. Smith, J. Matthiesen, and B. D. Kay, J. Phys. Chem. A **118**, 8242 (2014); D. V. Chakarov, L. Osterlund, and B. Kasemo, Vacuum **46**, 1109 (1995); P. Lofgren, P. Ahlstrom, D. V. Chakarov, J. Lausmaa, and B. Kasemo, Surf. Sci. **367**, L19 (1996); P. U. Andersson, M. T. Suter, N. Markovic, and J. B. C. Pettersson, J. Phys. Chem.

C **111**, 15258 (2007); X. R. Kong, P. U. Andersson, E. S. Thomson, and J. B. C. Pettersson, J. Phys. Chem. C **116**, 8964 (2012); P. Lofgren, P. Ahlstrom, J. Lausma, B. Kasemo, and D. Chakarov, Langmuir **19**, 265 (2003); R. Souda, Appl. Surf. Sci. **357**, 1809 (2015); J. Phys. Chem. C **121**, 12199 (2017); A. Politano, A. R. Marino, V. Formoso, and G. Chiarello, Carbon **49**, 5180 (2011).

[21] L. Lupi, A. Hudait, and V. Molinero, J. Am. Chem. Soc. **136**, 3156 (2014).

[22] L. Lupi, N. Kastelowitz, and V. Molinero, J. Chem. Phys. **141**, 18C508 (2014); T. Roman and A. Groß, J. Phys. Chem. C **120**, 13649 (2016); D. J. Anick, J. Phys. Chem. A **118**, 7498 (2014); P. C. Sanfelix, S. Holloway, K. W. Kolasinski, and G. R. Darling, Surf. Sci. **532**, 166 (2003).

[23] A. S. Bolina, A. J. Wolff, and W. A. Brown, J. Phys. Chem. B **109**, 16836 (2005).

[24] R. Souda, J. Phys. Chem. C **116**, 20895 (2012); J. Phys. Chem. B **110**, 17524 (2006); M. Luna, J. Colchero, and A. M. Baro, J. Phys. Chem. B **103**, 9576 (1999).

[25] See Supplemental Material at http://link.aps.org/supplemental/10.1103/PhysRevLett.121.256001 for details of the supporting information described in the text, supporting experiments, calculation details, definition of energy, 2D ice layers on various solid surfaces, and free-energy analysis, which include Refs. [26–44].

[26] J. VandeVondele, M. Krack, F. Mohamed, M. Parrinello, T. Chassaing, and J. Hutter, Comput. Phys. Commun. **167**, 103 (2005).

[27] A. D. Becke, Phys. Rev. A **38**, 3098 (1988).

[28] C. T. Lee, W. T. Yang, and R. G. Parr, Phys. Rev. B **37**, 785 (1988).

[29] S. Goedecker, M. Teter, and J. Hutter, Phys. Rev. B **54**, 1703 (1996).

[30] C. Hartwigsen, S. Goedecker, and J. Hutter, Phys. Rev. B **58**, 3641 (1998).

[31] S. Grimme, J. Antony, S. Ehrlich, and H. Krieg, J. Chem. Phys. **132**, 154104 (2010).

[32] S. Plimpton, J. Comput. Phys. **117**, 1 (1995).

[33] W. L. Jorgensen, J. Chandrasekhar, J. D. Madura, R. W. Impey, and M. L. Klein, J. Chem. Phys. **79**, 926 (1983).

[34] R. W. Hockney and J. W. Eastwood, *Computer Simulation Using Particles* (Adam Hilger, New York, 1989).

[35] E. H. Lieb, Phys. Rev. Lett. **18**, 692 (1967).

[36] S. T. Lin, M. Blanco, and W. A. Goddard, J. Chem. Phys. **119**, 11792 (2003).

[37] E. Fomin, M. Tatarkhanov, T. Mitsui, M. Rose, D. F. Ogletree, and M. Salmeron, Surf. Sci. **600**, 542 (2006).

[38] A. Beniya, Y. Sakaguchi, T. Narushima, K. Mukai, Y. Yamashita, S. Yoshimoto, and J. Yoshinobu, J. Chem. Phys. **130**, 034706 (2009).

[39] S. Haq, C. Clay, G. R. Darling, G. Zimbitas, and A. Hodgson, Phys. Rev. B **73**, 115414 (2006).

[40] S. Haq, J. Harnett, and A. Hodgson, Surf. Sci. **505**, 171 (2002).

[41] G. Zimbitas, S. Haq, and A. Hodgson, J. Chem. Phys. **123**, 174701 (2005).

[42] M. E. Gallagher, S. Haq, A. Omer, and A. Hodgson, Surf. Sci. **601**, 268 (2007).

[43] J. Hu, X. D. Xiao, D. F. Ogletree, and M. Salmeron, Science **268**, 267 (1995).

[44] M. Odelius, M. Bernasconi, and M. Parrinello, Phys. Rev. Lett. **78**, 2855 (1997).

[45] H. Geng, X. Liu, G. Shi, G. Bai, J. Ma, J. Chen, Z. Wu, Y. Song, H. Fang, and J. Wang, Angew. Chem., Int. Ed. **56**, 997 (2017).